Computation and Simulation of the Effect of Microstructures on Material Properties

W. Craig Carter
SMA Fellow, Advanced Materials for Micro- and Nano-Systems
Dept. of Materials Science and Engineering, Massachusetts Institute of Technology

Abstract— **Many material properties depend on specific details of microstructure and both optimal material performance and material reliability often correlate directly to microstructure. In nano- and micro-systems, the material's microstructure has a characteristic length scale that approaches that of the device in which it is used. Fundamental understanding and prediction of material behavior in nano- and micro-systems depend critically on methods for computing the effect of microstructure. Methods for including the physics and spatial attributes of microstructures are presented for a number of materials applications in devices. The research in our group includes applications of computation of macroscopic response of material microstructures, the development of methods for calculating microstructural evolution, and the morphological stability of structures. In this review, research highlights are presented for particular methods for computing the response in: 1) rechargeable lithium ion battery microstructures, 2) photonic composites with anisotropic particulate morphologies, 3) crack deflection in partially devitrified metallic glasses.**

I. Introduction

MICROSTRUCTURES influence many material properties and therefore have significant practical applications in the application of materials in devices and structures. In the general case, a material microstructure is a complex ensemble of crystalline materials in a large number of orientations, second phases, interfaces, and defects. The complexity of microstructures and their description is the origin of the difficulty of including their effect into the design of materials. Furthermore, practical problems of microstructural design for enhanced material properties is protracted by the lack of sufficient quantitative understanding of the role of microstructure in material properties. Our group consists of one professor, two postdocs, seven MIT and one SMA graduate student.[1] We do research on prediction, both computational and theoretical, of the effect of material microstructures on macroscopic properties and on the evolution of microstructure. Our research program at MIT and Singapore focuses on the quantification of microstructure, prediction of material properties from microstructural data, and the effect of materials processing on the evolution of microstructures in materials. We develop computational methods of computing that include microstructure and these methods are demonstrated to SMA students and used in their research.

This report focuses on those aspects of our research program that is directly related to our SMA activities. Dr. Rajesh Raghavan will be presenting his work on viscoelastic response of nanocomposite polymers in a separate document.

II. Microstructural Effects in Rechargeable Lithium Ion Batteries

Portable and reusable power supplies continue to be a critical materials need for developing technology.[2] Battery microstructures usually are micro- and/or nano-composites of ionic storage materials and ionic conductors. After a decade of development, the rechargeable lithium-ion battery occupies the prime position in the market place and the current (and potential) applications of lithium-ion batteries span laptops, hybrid cars, toys, cellular phones, etc. All these electronic appliances require an increasingly larger power and energy densities. Simultaneously, these devices require environmentally safe materials and large cycle-ability.

The minimum requirements for a typical rechargeable lithium-ion battery include operating voltages between 3 and 4 V, a voltage response constant in time (given a current drained current), and long shelf life (*i.e.*, the performance of a battery should not decay more than 10% in a ten years period). Finally, this device requires a wide operating temperature range that allows it to be utilized under the most stringent conditions [1].

A rechargeable battery is formed of three parts: Anode, cathode, and separator. The particular internal features of each part depend on the design and characteristics of the materials involved . During the charging and discharging (cycling) of a battery, the internal geometrical features of the cathode and anode (and any possible relevant features found on the separator) influence the local transport of Li-ions and electrons. These spatial inhomogeneities induce localized fluxes and gradients of concentration and voltage that ultimately control the macroscopic response of the system. In this context, study and understanding of the interrelation between the microstructure and properties during cycling of a battery become very important. In an attempt to understand and propose some criteria to improve the power and energy density of these systems, a

This research was supported by the Singapore-MIT Alliance.
W. Craig Carter is Associate Professor of Materials Science and Engineering at MIT, Room 13-5018, 77 Massachusetts Ave., Cambridge, MA 02139-4307 USA, 617-253-6048 ccarter@mit.edu http://pruffle.mit.edu/~ccarter/ .

[1]W. Craig Carter; Rajesh Raghavan and Andrew Reid; Catherine Bishop, Edwin Garcia, Martin Maldovan, Garry Maskalay, Ellen Siem, Andrew Takahashi, and Hao Wang; Lee Mei (Irene) Ling. Lee Mei Ling is co-supervised by Prof. Yi Li of NUS.

[2]The research in this section was performed by Edwin Garcia

model is proposed. This model is implemented by applying the Finite Element method to account for the physics and effect of microstructure of rechargeable batteries.

The properties of rechargeable lithium-ion batteries are determined by the electrochemical and kinetic properties of their constituent materials as well as by their underlying microstructure. In this past year, Edwin Garcia and I, in collaboration with Prof. Y.-M. Chiang, have developed a method that uses microscopic information and constitutive material properties to calculate the macroscopic response of rechargeable lithium-ion batteries. This analysis suggests four ways to improve performance of the $Li_yC_6|LiMn_2O_4$-based battery system: controlling the transport paths to the back of the cathode, maximizing the surface area for intercalating lithium ions, engineering the porosity of the electrolyte phase, and distributing the lithium ions evenly at the front of the cathode. Model battery microstructures were adapted from reference micrographs of Lithium-Oxide particulate cathodes [2] and appear in Figures 1 and 2.

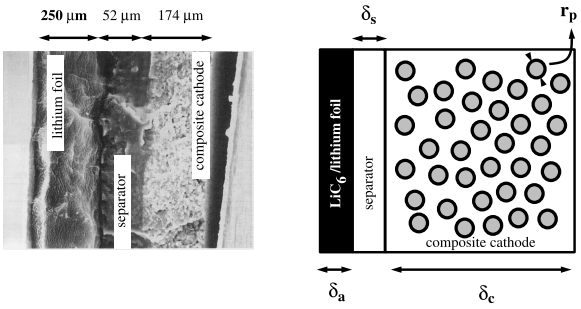

Fig. 1. Left, a micrograph showing a cross-section of a typical lithium ion rechargeable battery. Right, schematic depiction of the real system; δ_s is the separator thickness, δ_c the cathode thickness, δ_a the anode thickness, and r_p the typical particle radius.

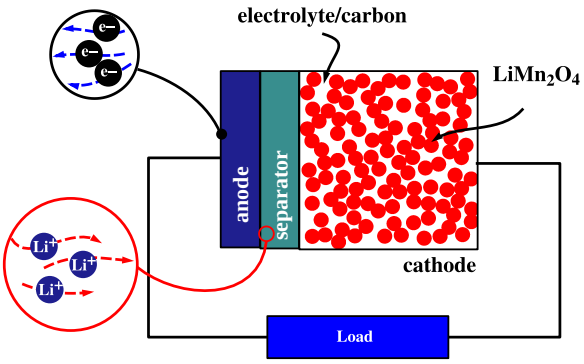

Fig. 2. Battery operation during galvanostatic discharge of a high energy density cathode. Externally, the ohmic load of resistance R induces a flux of electrons of magnitude $\Delta\phi/R$. Inside the battery, the flow of electrons results from the local oxidation/reduction processes. In the cathode, while the underlying thermodynamic properties determine the theoretical response of the device, the spatial distribution of $LiMn_2O_4$ particles and the kinetic properties define the macroscopic power and energy density.

A. Modeling of microstructural effects in Li-ion Batteries

A.1 Continuum Constitutive Behavior

The mass flux of Li-ions, $vecN_{Li}$, and charge current density, $\vec{J_q}$ are assumed to be linear functions of the Li gradient and electric field, $\vec{E} = -\nabla\phi$:

$$\begin{aligned} \vec{N_{Li}} &= -D_{Li}\nabla c_{Li} - M_{Li}c_{Li}\nabla\phi \\ \vec{J_q} &= -M_{Li}c_{Li}\nabla c_{Li} + M_e c_e \nabla c_e - \sigma_T \nabla\phi \end{aligned} \tag{1}$$

M^e_{Li} the electric ion mobility for ionized lithium, c_{Li} is the local concentration of lithium, and D_i the intrinsic diffusivity, and σ_T is the transference number.

Conservation and the assumption of no charge accumulation give:

$$\begin{aligned} \tfrac{\partial c_{Li}}{\partial t} &= \nabla\cdot(D_{Li}\nabla c_{Li}) + \nabla\cdot(M_{Li}c_{Li}\nabla\phi) \\ 0 &= \nabla\cdot(\sigma_T\nabla\phi) + \nabla\cdot(M_{Li}c_{Li}\nabla c_{Li}) \end{aligned} \tag{2}$$

Boundary conditions at the anode/electrolyte interface are given by empirical reaction kinetics that depend on the local over-potential η:

$$\vec{J}_q^{int} = \vec{J_q}\{e^{(\frac{\alpha_a F}{RT})\eta} - e^{-(\frac{\alpha_c F}{RT})\eta}\} \tag{3}$$

here the first term corresponds to the forward rate of the anodic process which is modulated by an empirical coefficient α_a. Likewise, α_c is the empirical parameter associated with the rate of the backward cathodic reaction. F is the Faraday constant, R is the gas constant, T is the absolute temperature, and η is the so-called local over-potential. Equation 3 is known as the *Butler-Volmer* equation. Physically, a particle-electrolyte interface that satisfies this equation would not allow exchange of lithium ions and electrons unless an over-potential $\eta \neq 0$ is induced at that particular point of the interface (*i.e.*, a required energetic penalty is applied for transference of the involved species). At equilibrium, the forward and backwards rate of reaction is effectively balanced, leading to an total charge current of *zero*.

The surface over-potential η is described by the proposed relation

$$\eta = (\Delta\phi - \phi_o) \tag{4}$$

ϕ_o is the so-called contact potential, z is the valence of the ionic species considered, and $\Delta\phi$ is the local voltage drop at the particle-electrolyte interface. Equation 3 describes the exchange of flux of charge between the particle and its surroundings, controlled by the electrochemical potential. In this particular case, the transfer of charged species is solely controlled by the over-potential, where ϕ_o may in the most arbitrary case depend on composition [3], [4].

A.2 Finite Element Modeling of Battery Microstructures

A finite element method for the solution of Equations 1—3 where the the diffusivity, mobility, transference number, and Butler-Volmer coefficients are determined by correlation to a specific microstructure through the OOF method [5], [6]. Simulations under constant discharge conditions were performed for cathode particulate microstructures by applying constant lithium flux at planar interface where the separator abuts the cathode.

The calculated time-dependence of Li-ion concentration and voltage distribution can be observed in Figures 3 and 4 for a simulated cathode microstructure. Properties and microstructural parameters were taken from Doyle [7]. Results suggest that the spatial distribution of $LiMn_2O_4$ particles, particle size, and boundary conditions influence power and energy density of the system. The results illustrate that some particles shield others on the back part (right) of the cathode, influencing and thus decreasing the power density of the overall device.

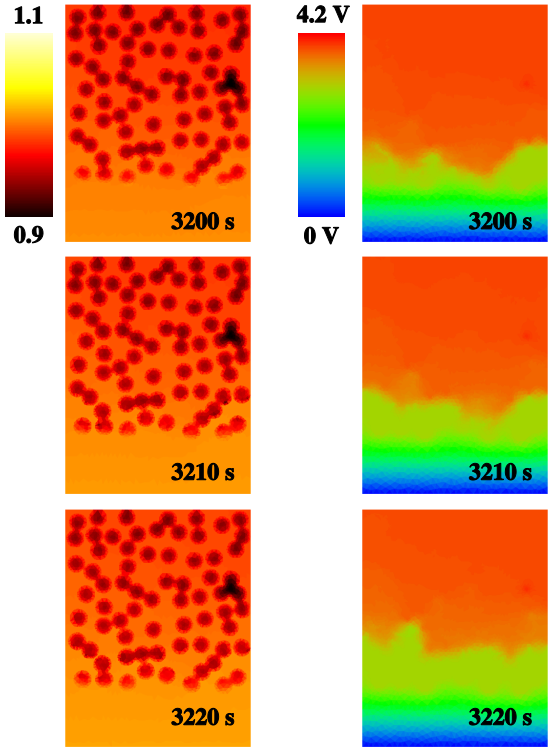

Fig. 4. The left column shows the distribution of lithium concentration at the end of discharge process for 1C. The right column shows the corresponding voltage. The battery is effectively discharged when the surface of the particles is saturated with lithium-ions, regardless if more lithium can be accommodated within each particle.

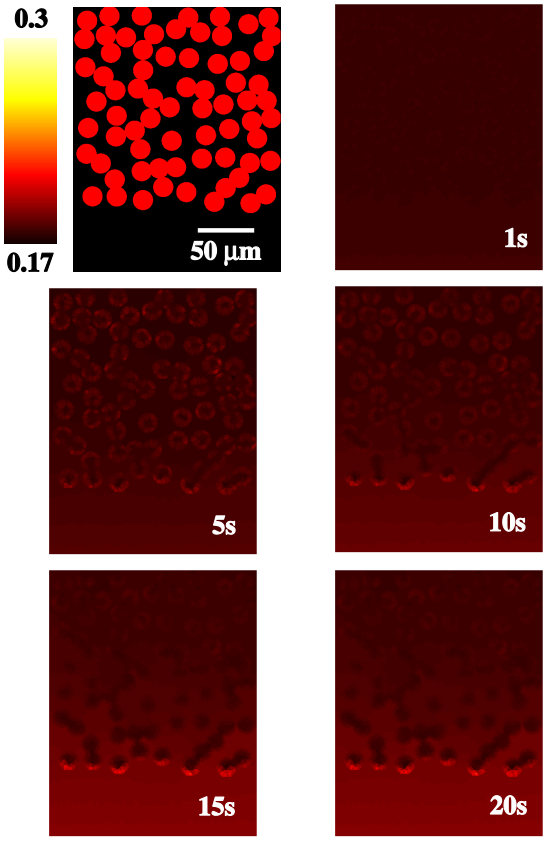

Fig. 3. Lithium distribution during the first twenty seconds of galvanostatic discharge. The sample microstructure and scale are shown on the top left. The battery is discharged under a load of 1C. Surface reaction kinetics are overcome by diffusion kinetics throughout the bulk of the cathode, except for those particles of $LiMn_2O_4$ that are closest to the anode.

The accumulative electric response from this device is summarized in the Ragone plot shown in Figure 5. Here, each power and energy density is a result of the predicted electric potential evolution and extracted current. The effect of the transport limitations is reflected in a rapidly decreasing energy density with increasing extracted power. The predicted battery performance agrees with the trends predicted by Doyle *et al.*, and Hellweg [7], [8], [9].

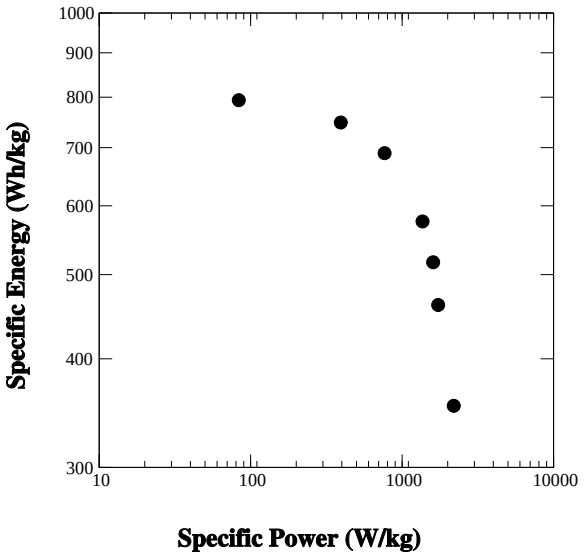

Fig. 5. Macroscopic energy density as a function of delivered power per unit mass (Ragone Plot). The predicted response corresponds to a cathode with randomly distributed particles of active material. Microstructure is shown in Figure 3.

The analyses suggest that the microstructure, anisotropy of the single-crystal properties, texture, and particle distribution can be engineered to match specific requirements in technological applications. For the $Li_yC_6|LiMn_2O_4$ battery system, the performance of the cathode is greatly improved if the lithium concentration is homogeneously distributed in the front and middle of the cathode. The response of the analyzed system is limited only by the transport processes occurring in the structureless anode.

In general, the demand of power and energy density in modern electronic appliances is always increasing. Consequently, improvement of electrode materials in rechargeable lithium-ion batteries is important. The analysis suggests that many potentially useful microstructural designs could be discovered through computational exploration. For example, different distributions of particle sizes or mixed phases of active host material in anode and cathode are just a few of several immediate possibilities for battery improvement through microstructural optimization. Furthermore, electrically and chemically induced phase transitions can be described by explicitly tracking the interface delimiting two (or more) stable phases or using a phase-field approach. Texture effects can be readily assessed. An important possible extension of this work consists including the detailed interactions between the anode and cathode section, *i.e.*, to study a rocking-chair configuration [2]. For all these instances, understanding of the properties and microstructural effects will yield an improvement of the device.

III. Effective Medium Approximations of Permittivity of Anisotropic Morphology Nano-Particle Dielectric Composites

The production of photonic devices depends on availability of materials with specific refractive indices.[3] When materials with appropriate refractive indices are not available, it is possible to engineer them with the incorporation of high index nano-particles into a low index host matrix [10], [11], *e.g.* the uniform spatial dissemination of polymer-grafted gold nano-particles within selected domains of di-block copolymer structures [10], [11], [12]. Additional dielectric control can be obtained by tuning the embedded nano-particle size and morphology optical properties. The resulting the photonic nanocomposite has a macroscopic "effective" dielectric constant that depends on the shape, volume fraction, and dielectric constant of the particles.

Martin Maldovan, in my research group, has developed models for the effect of size and morphology on effective dielectric media that are required for the design of photonic devices.

We present a method for calculating effective dielectric constants in composites with arbitrary particulate shape. The inherent accuracy of replacing a micro-architectural dielectric composite with a homogeneous effective medium is assessed by comparison of a finite element calculation that resolves individual particles in a particulate composite to one that treats the particulate composite as a uniform phase with homogeneous effective dielectric constant.

A. Effective Permittivity Model

A numerical representation of effective permittivity can be written

$$\varepsilon_{eff,i} = \varepsilon_m + \varepsilon_m \frac{f(\varepsilon_p - \varepsilon_m)\,\beta_i}{\varepsilon_m - L_{ii} f(\varepsilon_p - \varepsilon_m)\,\beta_i} \qquad (5)$$

where f is the particle filling fraction, and β_i is a constant that depends on particle shape and dielectric contrasts between the matrix and the particles.

β_i must be calculated for each particle morphology. In this report, the numerical constants are calculated for two-dimensional particle shapes for a sequence of dielectric configurations illustrated below. For each system, heterogeneous layers with illustrated geometries are used to calculate reflectivity by using the finite element method. Layer thicknesses are 120nm; mean particle separations are 30nm; filling fractions are 10%; n_{matrix}=1.5. $n_{particles}$=7.5.

Fig. 6. Circular nano-particles with larger dielectric constant embedded in a lower dielectric constant matrix. The numerical effective medium results can be compared to an analytic result for this case.

[3]The research in this section was performed by Martin Maldovan

Fig. 7. Square nano-particles with larger dielectric constant embedded in a lower dielectric constant matrix.

Fig. 8. Rectangles of aspect ratio 3:1 with long face normal to incidence radiation with larger dielectric constant embedded in a lower dielectric constant matrix.

Fig. 9. Rectangles of aspect ratio 1:3 with short face normal to incidence radiation with larger dielectric constant embedded in a lower dielectric constant matrix.

Fig. 10. Equilateral triangle nano-particles with vertex oriented towards incidence radiation with larger dielectric constant embedded in a lower dielectric constant matrix.

B. *Effective Permittivity Results*

The heterogeneous layers were meshed for finite element analysis of Maxwell's equations with incident plane-wave radiation from the left [13]. The effective medium constant, β, was determined from the numerical solution from Equation 5.

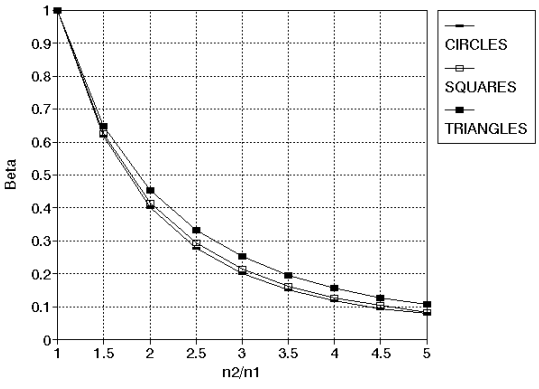

Fig. 11. Numerical FEM determination of β with equation 5 as a function of dielectric contrast between circular, square, and triangular nano-particles and matrix.

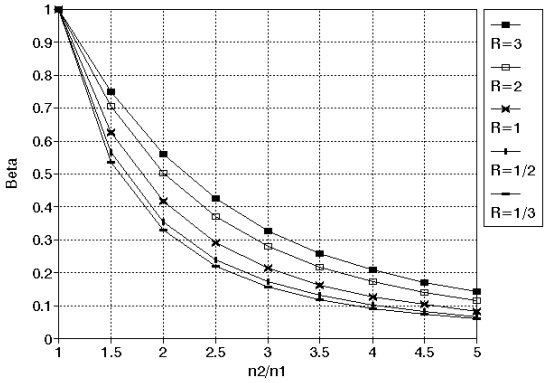

Fig. 12. Numerical FEM determination of β with equation 5 as a function of dielectric contrast between rectangular particles of various aspect ratios and matrix.

The reflectivity of layered structures can be calculated by the *transfer matrix method* (TMM) that treats the particle composite as an effective medium [14]. TMM is more approximate, but more numerically efficient, and would be preferred for calculation. Comparing the reflectivity from FEM for which accuracy is limited by numerical mesh resolution, but is numerically more difficult to implement, to the mean-field TMM is useful for the validation of comparative accuracy of the more efficient method. In all investigated geometries, the mean-field TMM calculations that treat the particulate layer as an effective medium with β calculated above cannot be distinguished from the FEM layer calculations that resolve the individual nanoparticles.

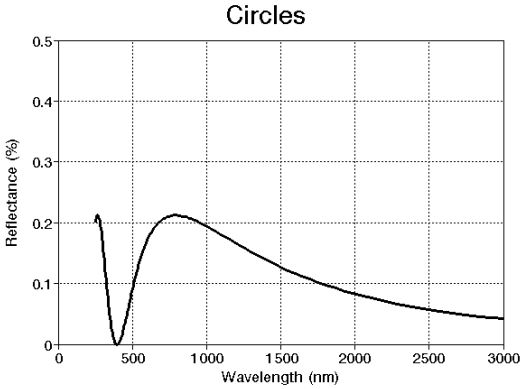

Fig. 13. Reflectivity versus incident wavelength for circular nano-particles, calculated by both FEM and effective medium TMM methods.

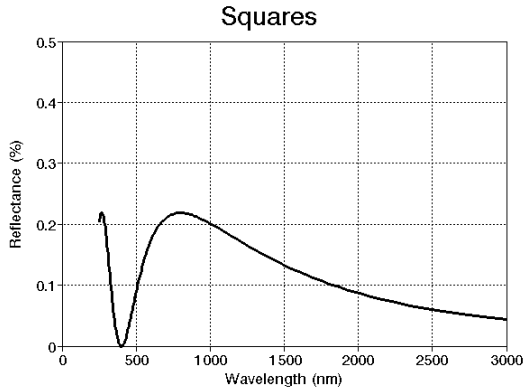

Fig. 14. Reflectivity versus incident wavelength for square nano-particles, calculated by both FEM and effective medium TMM methods.

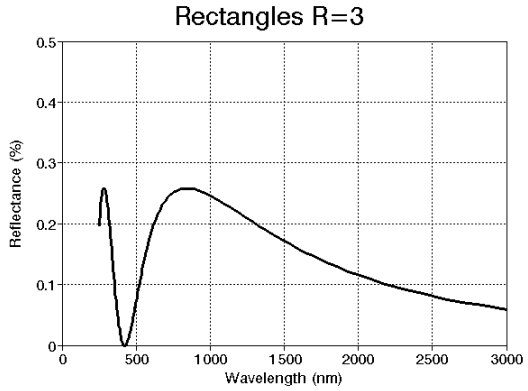

Fig. 15. Reflectivity versus incident wavelength for rectangular nano-particles of aspect ratio 3, calculated by both FEM and effective medium TMM methods.

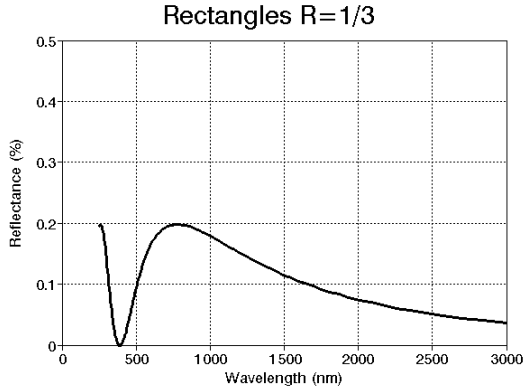

Fig. 16. Reflectivity versus incident wavelength for rectangular nano-particles of aspect ratio 1/3, calculated by both FEM and effective medium TMM methods.

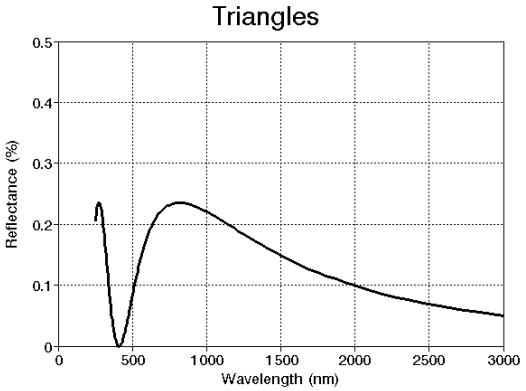

Fig. 17. Reflectivity versus incident wavelength for equilateral triangle nano-particles of aspect ratio 1/3, calculated by both FEM and effective medium TMM methods.

C. Conclusions for Effective Medium Methods for Nanophotonic Composites

Effective medium theory is a demonstrably accurate and potentially useful method for the rapid evaluation of a microcomposite's optical properties for various particle shapes because it eliminates extensive numerical calculations with tabulated values from a single numerical determination. Furthermore, numerical methods for extracting effective medium constants provide tools for evaluation of microcomposite 2-D photonic crystal designs. Comparison of the reflectivity values of a nanocomposite layer calculated using effective medium theory and the finite element method demonstrates that the effective medium approach is accurate within 1% for the properties of composite materials containing dielectric circular, square, rectangular, or triangular shaped particles.

IV. Microstructural Effects of Crack Deflection in Partially Devitrified Amorphous Metals

Bulk metallic glasses exhibit high yield strengths of approximately 2GPa and strain limit (2%) but have limited plastic deformation compared to polycrystalline metallic materials with similar compositions [15], [16].[4] Metallic glasses have been observed to deform by highly localized shear flow [15], [16]. The local plastic strain in each shear band is large; however, the overall strain is determined by the number of shear bands is an apparent upper limit of about 2%. This suggests that interactions between shear bands may play an important role in setting the toughness of amorphous metals. Loaded in a state of uniaxial or plane stress, metallic glasses fail catastrophically with one dominant shear band and show little plasticity—-the stress-strain curve is similar to that of a brittle material. Under constrained geometries (plane strain), amorphous metals fail in an elastic, perfectly plastic manner by the generation of multiple shear bands. Multiple shear bands

[4]The research in this section was performed by Lee Mei Ling

are observed under conditions of mechanical constraint, for example in uniaxial compression, bending, rolling, and under localized indentation. This quasi-brittle deformation behavior limits the application of bulk metallic glasses as an engineering material.

Bulk metallic glass matrix composites with ductile metal or refractory ceramic particles as reinforcements have improved toughness [17], [18]. One proposed explanation for the increase in toughness is that the particles restrict shear bands propagation and promote the generation of multiple shear bands. This opens the possibility of producing an entirely new class of materials which combine the high strength of metallic glass with the ability to undergo plastic deformation under confined or otherwise unstable loading conditions.

Engineering design of metallic glass matrix composites has raised issues regarding the optimal value of volume fraction and types of crystalline phases that could be incorporated into an amorphous matrix and enhance toughness without being detrimental to the mechanical performance and the deformation mechanisms controlling the composite's properties.

Microstructural simulations of the effect of second phase particles on the production of multiple shear bands can be used to investigate the influence of second phase particles and begin a search for optimal combinations of properties and microstructural features.

The OOF [5], [6] microstructural simulation program is being used to develop models for microstructural interactions between the second phases in the amorphous matrix with the propagation of the shear bands under different deformation modes by performing virtual tests.

The microstructural simulations are being used to study the interaction between the second phase and the propagation of shear bands and find the combination of volume fraction, distribution, type and properties of the second phase that can enhanced the properties of metallic glasses and the deformation mechanisms controlling the composite's properties

We plan to correlate the computational result with experimental result and consider how these mechanisms interact with hypothetical and observed microstructures.

A. *Microstructural Effects in Shear Band Multiplication: Preliminary Results*

Due to the complexity of the fracture behavior of metallic glasses, simple microstructures are modeled so that fundamental mechanisms of multiple shear band generation can be identified for further study.

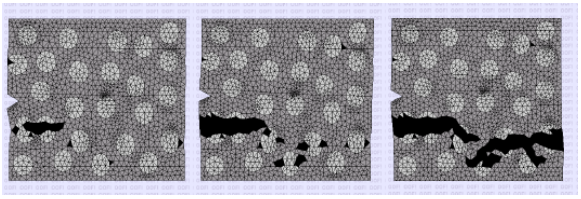

Fig. 18. Illustration of a model system that has been meshed with properties that reflect the underlying microstructure. This initial numerical experiment illustrates the propagation of shear bands from an initial notch through a matrix with softer elastic particles. The particle shear band propagation resistance is about 1/10m that of the matrix.

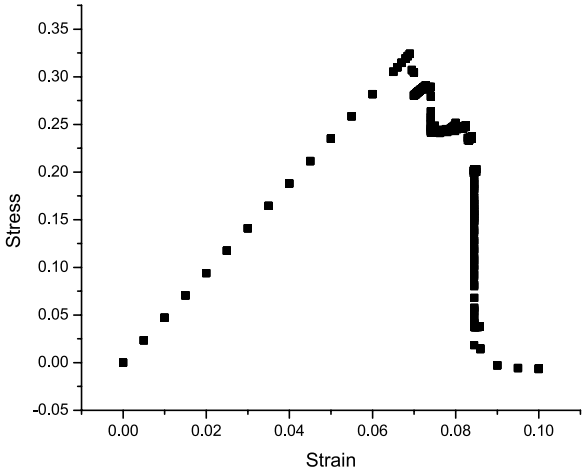

Fig. 19. Illustration of stress-strain results illustrating the damage accumulation from experiments like that illustrated in Fig. 18.

References

[1] Colin A. Vincent, "Lithium Batteries:a 50-year Perspective, 1959-2009," *Solid State Ionics*, vol. 134, pp. 159–167, 2002.

[2] Colin A. Vincent and Bruno Scrosati, *Modern Batteries. An Introduction to Electrochemical Power Sources*, John Wiley and Sons, New York, 1997.

[3] Allen J. Bard and Larry R. Faulkner, *Electrochemical Methods. Fundamentals and Applications*, John Wiley and Sons, Inc., New York, 1980.

[4] John S. Newman, *Electrochemical Systems*, Prentice Hall International, Englewood Cliffs, New Jersey 07632, 1980.

[5] W. Craig Carter and Stephen A. Langer, *The OOF Manual: Version 1.0*, National Intitute of Standards and Technology, 100 Bureau Drive, Stop 8910; Gaithersburg MD, USA, nistir 6256 edition, 1998, http://www.ctcms.nist.gov/oof/.

[6] Langer S. A, Fuller E., and Carter W. C., "Oof: An image-based finite-element analysis of material microstructures," *Computing in Science and Engineering*, vol. 3, pp. 15–23, 2001.

[7] Christopher Marc Doyle, *Design and Simulation of Lithium Rechargeable Batteries*, Ph.D. thesis, Department of Chemical Engineering. University of California at Berkeley, 1995.

[8] Benjamin Hellweg, "Microstructural Modeling of Lithium Battery Electrodes," M.S. thesis, Department of Materials Science and Engineering, Massachusetts Institute of Technology, 2000.

[9] Marc Doyle, Thomas F. Fuller, and John Newman, "The Importance of the Lithium Ion Transference Number in Lithium/Polymer Cells," *Electrochemica Acta*, vol. 39, pp. 2073–2081, 1994.

[10] R. Pelster and U. Simon, "Nanodispersions of conducting particles:preparation, microstructure and dielectric properties," *Colloid Polym. Sci.*, vol. 277, pp. 2–14, 1999.

[11] W. Caseri, "Nanocomposites of polymers and metals or semicon-

ductors: Historical background and optical properties," *Macromol. Rapid Commun.*, vol. 21, pp. 705–722, 2000.

[12] Bockstaller M, Kolb R, and Thomas EL, "Metallodielectric photonic crystals based on diblock copolymers," *Adv. Mater.*, vol. 13, pp. 1783–1786, 2001.

[13] Volakis JL, *Finite element method for electromagnetics : antennas, microwave circuits, and scattering applications*, IEEE Press, New York, 1998.

[14] Yeh P, Yariv A, and Hong CS, "Electromagnetic propagation in periodic stratified media 1. general theory," *J. Opt. Soc. Am.*, vol. 67, pp. 423–448, 1977.

[15] H.S. Chen, H.J. Leamy, and M. J. O'Brien, "Bending deformation in metallic glasses," *Scripa Metall Mater*, vol. 7, pp. 415–419, 1973.

[16] Takayama S and Maddin R, "Fracture of amorphous ni-pd-p alloys," *Phil. Mag*, vol. 32, pp. 457–470, 1975.

[17] Conner RD, Choi-Yim H, and Johnson WL, "Mechanical properties of zr57nb5al10cu15.4ni12.6 metallic glass matrix particulate composites," *J. Mater. Res.*, vol. 14, pp. 3292–3297, 1999.

[18] Hays CC, Kim CP, and Johnson WL, "Microstructure controlled shear band pattern formation and enhanced plasticity of bulk metallic glasses containing in situ formed ductile phase dendrite dispersions," *Phys Rev Lett*, vol. 84, pp. 2901–2904, 2002.